A Transversely Isotropic Magneto-electro-elastic Circular Kirchhoff Plate Model Incorporating Microstructure Effect

Wei Shen, Gongye Zhang, Shuitao Gu, Yu Cong

A Transversely Isotropic Magneto-electro-elastic Circular Kirchhoff Plate Model Incorporating Microstructure Effect

Wei Shen[1] Gongye Zhang[2,*] Shuitao Gu[1,] Yu Cong[3]**

([1] School of Civil Engineering, Chongqing University, Chongqing 400044, China)
([2] Jiangsu Key Laboratory of Engineering Mechanics, School of Civil Engineering, Southeast University, Nanjing 210096, China)
([3] University Paris-Saclay, Univ Evry, LMEE, 91020, Evry, France)

ABSTRACT A non-classical model for transversely isotropic magneto-electro-elastic circular Kirchhoff plates is established based on the extended modified couple stress theory. The Gibbs-type variational principle is used to obtain the governing equations and boundary conditions. To illustrate the newly derived model, the static bending problem of a clamped circular plate subjected to a uniformly distributed constant load is solved numerically by Fourier–Bessel series. The numerical results show that the values of transverse displacement, electric and magnetic potentials predicted by the current model are always smaller than those of the classical model, and the differences are diminishing as the plate thickness increases. In addition, it is shown that the magneto-electro-elastic coupling effect plays an important role in the transverse displacement, electric potential and magnetic potential of the magneto-electro-elastic circular Kirchhoff plates. Furthermore, several reduced specific models are provided for simpler cases.

KEY WORDS Circular Kirchhoff plate, Magneto-electro-elastic plate, Microstructure effect, Couple stress theory, Static bending

* Corresponding author. E-mail: gyzhang@seu.edu.cn (G. Y. Zhang).
** Corresponding author. E-mail: gust@cqu.edu.cn (S. T. Gu).

1. Introduction

Due to the piezomagnetic/piezoelectric/magnetoelectric effect, thin plates made of magneto-electro-elastic (MEE) materials are able to realize the mutual conversion between magnetic, electric and mechanical energies. Such characteristics have found significant applications in sensors, resonators, energy harvesters, semiconductors and other systems [1-6]. It is observed that these thin plates exhibit microstructure-dependent size effects at the micron and nanometer scales [7-9]. Owing to the lack of any size-dependent material parameter [10], classical elasticity theories cannot effectively describe such size effects. Hence, higher-order elasticity theories that contain additional parameters should be introduced to develop models for thin MEE plates considering microstructure-dependent size effects.

Several studies for MEE plates using higher-order elasticity theories have been completed. For instance, a non-local constitutive relation proposed by Eringen [11, 12] has been used to develop a model for the MEE Mindlin plate (i.e., Li et al. [13]). Vinyas et al. [14] addressed a free vibration problem of skew MEE plates by employing Reddy's third-order shear deformation theory (e.g. [15]). Zheng et al. [16] also applied Reddy's high-order shear deformation theory and combined von Karman's nonlinear geometric equation to analyze the nonlinear bending of MEE plates. Wang et al. [17] established a model for MEE plates considering both nonlocal and surface effects. Ebrahimi and Dabbagh [18] developed a model for MEE nanoplates via a nonlocal strain gradient theory to capture size effects. Qu et al. [19] developed a new anisotropic MEE Mindlin plate model by using an extended

modified couple stress theory.

Different from the classical couple stress theory [20-22], the modified couple stress theory [23, 24] and its extended version [19, 25, 26] only consider the symmetric part of the curvature tensor conjugated with the deviatoric part of the couple stress tensor, which contain fewer material length scale parameters than the classical counterparts. Considering the difficulties in determining additional material parameters and the physical interpretation of the microstructure, these modified theories have been successfully employed to develop non-classical beam and plate models [19, 25-29]. Because of the complexity of cylindrical coordinates in mathematics, little research has been done on circular plates. However, due to the special geometry of circular and annular plates, circular MEE plates are often used in a wide range of engineering applications. Hence, a model for transversely isotropic MEE circular Kirchhoff plates at very small scale and can capture microstructure effect is very desirable.

The current work aims to develop a microstructure-dependent transversely isotropic MEE model for circular Kirchhoff plates. The rest of the paper is organized as follows. In Section 2, a new model is established through a variational method by using the extended modified couple stress theory. In Section 3, several special cases are provided. In Section 4, the static bending problem of a clamped circular plate subject to a uniformly distributed constant load is solved by applying the formulas in Section 2 through Fourier–Bessel series. The paper concludes in Section 5 with a summary.

2. Formulation

Figure 1 shows an annular circular thin plate of uniform thickness h, inner radius a and outer radius b. The displacement field in such a circular Kirchhoff plate can be written in the form of the cylindrical coordinate system as [28]

$$u_r(r,\theta,z) = u(r) - z\frac{\partial w(r)}{\partial r} \tag{1a}$$

$$u_\theta(r,\theta,z) = 0 \tag{1b}$$

$$u_z(r,\theta,z) = w(r) \tag{1c}$$

where u_r, u_θ and u_z are, respectively, the radial, tangential and transverse components of the displacement vector **u**. u and w are, respectively, the radial and transverse components of the displacement vector of point on the mid-plane of the plate.

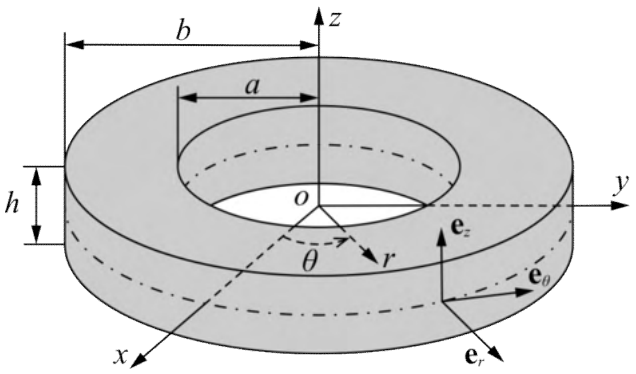

Fig. 1. The annular circular thin plate's geometry and coordinate system

According to the work of Zhang et al. [26] and Wang [30], the electric and magnetic potentials in such a Kirchhoff plate can be written as

$$\Phi(r,\theta,z) = -\cos\left(\frac{\pi}{h}z\right)\gamma(r) + \frac{2z}{h}\gamma_0 \tag{2a}$$

$$M(r,\theta,z) = -\cos\left(\frac{\pi}{h}z\right)\zeta(r) + \frac{2z}{h}\zeta_0 \tag{2b}$$

where Φ represents the electric potential, and M represents the magnetic potential. γ

and ζ represent the spatial variations of electric potential and magnetic potential on the mid-plane, respectively. γ_0 and ζ_0 denote the external electric potential and magnetic potential, respectively.

The constitutive equations considering the extended version of modified couple stress theory for transversely isotropic MEE materials can be expressed as [19, 26]

$$\begin{Bmatrix}\sigma_{rr}\\ \sigma_{\theta\theta}\\ \sigma_{zz}\\ \sigma_{\theta z}\\ \sigma_{zr}\\ \sigma_{r\theta}\end{Bmatrix}=\begin{bmatrix}C_{11} & C_{12} & C_{13} & 0 & 0 & 0\\ C_{12} & C_{11} & C_{13} & 0 & 0 & 0\\ C_{13} & C_{13} & C_{33} & 0 & 0 & 0\\ 0 & 0 & 0 & C_{44} & 0 & 0\\ 0 & 0 & 0 & 0 & C_{44} & 0\\ 0 & 0 & 0 & 0 & 0 & \dfrac{C_{11}-C_{12}}{2}\end{bmatrix}\begin{Bmatrix}\varepsilon_{rr}\\ \varepsilon_{\theta\theta}\\ \varepsilon_{zz}\\ 2\varepsilon_{\theta z}\\ 2\varepsilon_{zr}\\ 2\varepsilon_{r\theta}\end{Bmatrix}$$
$$-\begin{bmatrix}0 & 0 & e_{31}\\ 0 & 0 & e_{31}\\ 0 & 0 & e_{33}\\ 0 & e_{15} & 0\\ e_{15} & 0 & 0\\ 0 & 0 & 0\end{bmatrix}\begin{Bmatrix}E_r\\ E_\theta\\ E_z\end{Bmatrix}-\begin{bmatrix}0 & 0 & q_{31}\\ 0 & 0 & q_{31}\\ 0 & 0 & q_{33}\\ 0 & q_{15} & 0\\ q_{15} & 0 & 0\\ 0 & 0 & 0\end{bmatrix}\begin{Bmatrix}H_r\\ H_\theta\\ H_z\end{Bmatrix} \tag{3a}$$

$$\begin{Bmatrix}m_{rr}\\ m_{\theta\theta}\\ m_{zz}\\ m_{\theta z}\\ m_{zr}\\ m_{r\theta}\end{Bmatrix}=\begin{bmatrix}A_{11} & A_{12} & A_{13} & 0 & 0 & 0\\ A_{12} & A_{11} & A_{13} & 0 & 0 & 0\\ A_{13} & A_{13} & A_{33} & 0 & 0 & 0\\ 0 & 0 & 0 & A_{44} & 0 & 0\\ 0 & 0 & 0 & 0 & A_{44} & 0\\ 0 & 0 & 0 & 0 & 0 & \dfrac{A_{11}-A_{12}}{2}\end{bmatrix}\begin{Bmatrix}\chi_{rr}\\ \chi_{\theta\theta}\\ \chi_{zz}\\ 2\chi_{\theta z}\\ 2\chi_{zr}\\ 2\chi_{r\theta}\end{Bmatrix} \tag{3b}$$

$$\begin{Bmatrix}D_r\\ D_\theta\\ D_z\end{Bmatrix}=\begin{bmatrix}0 & 0 & 0 & 0 & e_{15} & 0\\ 0 & 0 & 0 & e_{15} & 0 & 0\\ e_{31} & e_{31} & e_{33} & 0 & 0 & 0\end{bmatrix}\begin{Bmatrix}\varepsilon_{rr}\\ \varepsilon_{\theta\theta}\\ \varepsilon_{zz}\\ 2\varepsilon_{\theta z}\\ 2\varepsilon_{zr}\\ 2\varepsilon_{r\theta}\end{Bmatrix}$$

$$+\begin{bmatrix} \epsilon_{11} & 0 & 0 \\ 0 & \epsilon_{11} & 0 \\ 0 & 0 & \epsilon_{33} \end{bmatrix}\begin{Bmatrix} E_r \\ E_\theta \\ E_z \end{Bmatrix}+\begin{bmatrix} d_{11} & 0 & 0 \\ 0 & d_{11} & 0 \\ 0 & 0 & d_{33} \end{bmatrix}\begin{Bmatrix} H_r \\ H_\theta \\ H_z \end{Bmatrix} \tag{3c}$$

$$\begin{Bmatrix} B_r \\ B_\theta \\ B_z \end{Bmatrix}=\begin{bmatrix} 0 & 0 & 0 & 0 & q_{15} & 0 \\ 0 & 0 & 0 & q_{15} & 0 & 0 \\ q_{31} & q_{31} & q_{33} & 0 & 0 & 0 \end{bmatrix}\begin{pmatrix} \varepsilon_{rr} \\ \varepsilon_{\theta\theta} \\ \varepsilon_{zz} \\ 2\varepsilon_{\theta z} \\ 2\varepsilon_{zr} \\ 2\varepsilon_{r\theta} \end{pmatrix}$$

$$+\begin{bmatrix} \mu_{11} & 0 & 0 \\ 0 & \mu_{11} & 0 \\ 0 & 0 & \mu_{33} \end{bmatrix}\begin{Bmatrix} H_r \\ H_\theta \\ H_z \end{Bmatrix}+\begin{bmatrix} d_{11} & 0 & 0 \\ 0 & d_{11} & 0 \\ 0 & 0 & d_{33} \end{bmatrix}\begin{Bmatrix} E_r \\ E_\theta \\ E_z \end{Bmatrix} \tag{3d}$$

where σ_{ij} are the Cauchy stresses, m_{ij} are the couple stresses, D_i are the electric displacements, B_i are the magnetic fluxes. C_{ij} and A_{ij} denote the components of the elastic stiffness tensor and the couple stress stiffness tensor, respectively. e_{ij} and q_{ij} denote the piezoelectric and piezomagnetic tensors, respectively. ϵ_{ij}, d_{ij} and μ_{ij} denote the components of the dielectric tensors, magneto-dielectric tensors and magnetic permeability tensors, respectively. ε_{ij} and χ_{ij} are, respectively, the components of strain and curvature tensors defined by

$$\boldsymbol{\varepsilon}=\frac{1}{2}\left[\nabla\boldsymbol{u}+\left(\nabla\boldsymbol{u}\right)^{\mathrm{T}}\right] \tag{4a}$$

$$\boldsymbol{\chi}=\frac{1}{2}\left[\nabla\boldsymbol{\psi}+\left(\nabla\boldsymbol{\psi}\right)^{\mathrm{T}}\right] \tag{4b}$$

with $\boldsymbol{\psi}$ being

$$\boldsymbol{\psi}=\frac{1}{2}\mathrm{c\ u\ r}\boldsymbol{u} \tag{4c}$$

in which, $\boldsymbol{u}$ is the displacement vector, ∇ denotes the gradient, and the superscript T represents the transpose. In addition, the components of the electric field intensity E_i and the magnetic field intensity H_i are given by

$$\boldsymbol{E}=-\nabla\boldsymbol{\Phi},\quad \boldsymbol{H}=-\nabla\boldsymbol{M} \tag{5a, b}$$

It follows from Eqs. (1a-c), (2a, b), (4a-c) and (5a, b) that in the current Kirchhoff plate

$$\varepsilon_{rr}=\frac{\partial u}{\partial r}-z\frac{\partial^2 w}{\partial r^2},\ \varepsilon_{\theta\theta}=\frac{1}{r}\left(u-z\frac{\partial w}{\partial r}\right),\ \varepsilon_{zz}=\varepsilon_{r\theta}=\varepsilon_{zr}=\varepsilon_{z\theta}=0 \tag{6a}$$

$$\chi_{r\theta}=\chi_{\theta r}=-\frac{1}{2}r\frac{\partial}{\partial r}\left(\frac{1}{r}\frac{\partial w}{\partial r}\right),\ \chi_{rr}=\chi_{\theta\theta}=\chi_{zz}=\chi_{rz}=\chi_{\theta z}=0 \tag{6b}$$

$$E_r=\cos\left(\frac{\pi}{h}z\right)\frac{\partial\gamma}{\partial r},\ E_\theta=0,\ E_z=-\frac{\pi}{h}\sin\left(\frac{\pi}{h}z\right)\gamma-\frac{2\gamma_0}{h} \tag{6c}$$

$$H_r=\cos\left(\frac{\pi}{h}z\right)\frac{\partial\zeta}{\partial r},\ H_\theta=0,\ H_z=-\frac{\pi}{h}\sin\left(\frac{\pi}{h}z\right)\zeta-\frac{2\zeta_0}{h} \tag{6d}$$

The first variation of the Gibbs-type energy for the deformed MEE Kirchhoff plate is given by [31]

$$\delta U=\int_\Omega\left(\sigma_{ij}\delta\varepsilon_{ij}+m_{ij}\delta\chi_{ij}-D_i\delta E_i-B_i\delta H_i\right)\mathrm{d}V \tag{7}$$

where Ω is the volume of the plate, and

$$\begin{aligned}&\int_\Omega\left(\sigma_{ij}\delta\varepsilon_{ij}+m_{ij}\delta\chi_{ij}\right)\mathrm{d}V=\int_\Omega\left(\sigma_{rr}\delta\varepsilon_{rr}+\sigma_{\theta\theta}\delta\varepsilon_{\theta\theta}+2m_{r\theta}\delta\chi_{r\theta}\right)\mathrm{d}V\\&=\int_0^{2\pi}\int_a^b\left[\left(N_{\theta\theta}-\frac{\partial rN_{rr}}{\partial r}\right)\delta u+\left(\frac{\partial M_{\theta\theta}}{\partial r}-\frac{\partial^2 rM_{rr}}{\partial r^2}-3\frac{\partial Y_{r\theta}}{\partial r}-r\frac{\partial^2 Y_{r\theta}}{\partial r^2}\right)\delta w\right]\mathrm{d}r\mathrm{d}\theta\\&+\int_0^{2\pi}\left[rN_{rr}\delta u+\left(\frac{\partial rM_{rr}}{\partial r}-M_{\theta\theta}+2Y_{r\theta}+r\frac{\partial Y_{r\theta}}{\partial r}\right)\delta w-\left(rM_{rr}+rY_{r\theta}\right)\frac{\partial\delta w}{\partial r}\right]\Bigg|_a^b\mathrm{d}\theta\end{aligned} \tag{8}$$

$$\begin{aligned}&N_{\theta\theta}=\int_{-h/2}^{h/2}\sigma_{\theta\theta}\mathrm{d}z,N_{rr}=\int_{-h/2}^{h/2}\sigma_{rr}\mathrm{d}z,M_{rr}=\int_{-h/2}^{h/2}\sigma_{rr}z\mathrm{d}z\\&M_{\theta\theta}=\int_{-h/2}^{h/2}\sigma_{\theta\theta}z\mathrm{d}z,Y_{r\theta}=\int_{-h/2}^{h/2}m_{r\theta}\mathrm{d}z\end{aligned} \tag{9a-e}$$

$$\begin{aligned}&\int_\Omega D_i\delta E_i\ \mathrm{d}V=\int_\Omega\left(D_r\delta E_r+D_\theta\delta E_\theta+D_z\delta E_z\right)\mathrm{d}V\\&=\int_0^{2\pi}\int_a^b\left(-\frac{\partial r\Xi_r}{\partial r}\delta\gamma-r\Xi_z\delta\gamma\right)\mathrm{d}r\mathrm{d}\theta+\int_0^{2\pi}\left(r\Xi_r\delta\gamma\right)\Big|_a^b\mathrm{d}\theta\end{aligned} \tag{10}$$

$$\Xi_r = \int_{-h/2}^{h/2} D_r \cos\left(\frac{\pi}{h} z\right) \mathrm{d}z,\ \Xi_z = \int_{-h/2}^{h/2} D_z \frac{\pi}{h} \sin\left(\frac{\pi}{h} z\right) \mathrm{d}z \tag{11a, b}$$

$$\begin{aligned} \int_\Omega B_i \delta H_i \ \mathrm{d}V &= \int_\Omega \left(B_r \delta H_r + B_\theta \delta H_\theta + B_z H_z\right) \mathrm{d}V \\ &= \int_0^{2\pi} \int_a^b \left(-\frac{\partial r \Sigma_r}{\partial r} \delta\zeta - r\Sigma_z \delta\gamma\right) \mathrm{d}r\mathrm{d}\theta + \int_0^{2\pi} \left(r\Sigma_r \delta\zeta\right)\Big|_a^b \ \mathrm{d}\theta \end{aligned} \tag{12}$$

$$\Sigma_r = \int_{-h/2}^{h/2} B_r \cos\left(\frac{\pi}{h} z\right) \mathrm{d}z, \Sigma_z = \int_{-h/2}^{h/2} B_z \frac{\pi}{h} \sin\left(\frac{\pi}{h} z\right) \mathrm{d}z \tag{13a, b}$$

Note that Eqs. (8, 9) stand for the elastic part of the first variation of the Gibbs-type energy, while Eqs. (10, 11) and Eqs. (12, 13) represent the electric potential-related and magnetic potential-related parts, respectively.

The first variation of the virtual work (with $c_\theta = 0$) can be obtained as [27, 28]

$$\delta W = \int_0^{2\pi} \int_a^b \left(r f_r \delta u + r f_z \delta w \delta w\right) \mathrm{d}r\mathrm{d}\theta + \int_0^{2\pi} \left(r \bar{t}_r \delta u - r \bar{M}_\theta \frac{\partial \delta w}{\partial r} + r \bar{t}_z \delta w\right)\Big|_a^b \ \mathrm{d}\theta \tag{14}$$

where f_i is the body force resultant (force per unit area) of the i-direction, t_i is the Cauchy traction resultant (force per unit length) of the i-direction, and $\bar{M}_\theta$ is the applied moment per unit arc length along the circular boundary.

Applying the Gibbs-type variational principle and the fundamental lemma of the calculus of variations [31], the governing equations result in

$$h C_{11} \frac{\mathrm{d}}{\mathrm{d}r}\left[\frac{1}{r}\frac{\mathrm{d}}{\mathrm{d}r}\left(ru\right)\right] + f_r = 0 \tag{15a}$$

$$-\left[\frac{h^3}{12} C_{11} + \frac{h}{2}\left(A_{11} - A_{12}\right)\right] \nabla^4 w + \frac{2h}{\pi} e_{31} \nabla^2 \gamma + \frac{2h}{\pi} q_{31} \nabla^2 \zeta + f_z = 0 \tag{15b}$$

$$\frac{h}{2} \epsilon_{11} \nabla^2 \gamma + \frac{h}{2} d_{11} \nabla^2 \zeta - 2 e_{31} \frac{h}{\pi} \nabla^2 w - \frac{\pi^2}{2h} \epsilon_{33} \gamma - \frac{\pi^2}{2h} d_{33} \zeta = 0 \tag{15c}$$

$$\frac{h}{2} \mu_{11} \nabla^2 \zeta + \frac{h}{2} d_{11} \nabla^2 \gamma - 2 q_{31} \frac{h}{\pi} \nabla^2 w - \frac{\pi^2}{2h} \mu_{33} \zeta - \frac{\pi^2}{2h} d_{33} \gamma = 0 \tag{15d}$$

and the boundary conditions yield

$$hC_{11}\frac{\partial u}{\partial r}+\frac{h}{r}C_{12}u+2e_{31}\gamma_0+2q_{31}\zeta_0-\bar{t}_r=0 \tag{16a}$$

or $u=\bar{u}$ at $r=a$ and $r=b$,

$$\left[\frac{h^3}{12}C_{11}+\frac{h}{2}\left(A_{11}-A_{12}\right)\right]\frac{\partial}{\partial r}\nabla^2 w-\frac{2h}{\pi}e_{31}\frac{\partial\gamma}{\partial r}-\frac{2h}{\pi}q_{31}\frac{\partial\zeta}{\partial r}+\bar{t}_z=0 \tag{16b}$$

or $w=\bar{w}$ at $r=a$ and $r=b$,

$$\epsilon_{11}\frac{\partial\gamma}{\partial r}+d_{11}\frac{\partial\zeta}{\partial r}=0 \quad \text{or} \quad \gamma=\bar{\gamma} \text{ at } r=a \text{ and } r=b \tag{16c}$$

$$\mu_{11}\frac{\partial\zeta}{\partial r}+d_{11}\frac{\partial\gamma}{\partial r}=0 \quad \text{or} \quad \zeta=\bar{\zeta} \text{ at } r=a \text{ and } r=b \tag{16d}$$

$$\begin{aligned}&-\frac{h^3}{12}C_{11}\frac{\partial^2 w}{\partial r^2}-\frac{h^3}{12r}C_{12}\frac{\partial w}{\partial r}+\frac{2h}{\pi}e_{31}\gamma+\frac{2h}{\pi}q_{31}\zeta-\frac{h}{2}\left(A_{11}-A_{12}\right)\nabla^2 w\\&-\bar{M}_\theta=0 \quad \text{or} \quad \frac{\partial w}{\partial r}=\frac{\partial\bar{w}}{\partial r} \text{ at } r=a \text{ and } r=b\end{aligned} \tag{16e}$$

where

$$\nabla^2=\frac{1}{r}\frac{\partial}{\partial r}\left(r\frac{\partial}{\partial r}\right),\ \nabla^4=\frac{1}{r}\frac{\partial}{\partial r}\left\{r\frac{\partial}{\partial r}\left[\frac{1}{r}\frac{\partial}{\partial r}\left(r\frac{\partial}{\partial r}\right)\right]\right\} \tag{17}$$

3. Specific Models

In this section, a few specific models reduced from the current non-classical transversely isotropic MEE circular Kirchhoff plate model developed in Section 2 are provided.

3.1. Transversely Isotropic Piezoelectric Circular Kirchhoff Plate Model Incorporating the Microstructure Effect

When the piezomagnetic effect is neglected by setting $q_{ij}= 0$, $\mu_{ij}= 0$ and $d_{ij}= 0$, Eqs. (15a-d) reduce to

$$hC_{11}\frac{d}{dr}\left[\frac{1}{r}\frac{\mathrm{d}}{\mathrm{d}r}(ru)\right]+f_r=0 \tag{18a}$$

$$-\left[\frac{h^3}{12}C_{11}+\frac{h}{2}\left(A_{11}-A_{12}\right)\right]\nabla^4 w+\frac{2h}{\pi}e_{31}\nabla^2\gamma+f_z=0 \tag{18b}$$

$$\frac{h}{2}\epsilon_{11}\nabla^2\gamma-2e_{31}\frac{h}{\pi}\nabla^2 w-\frac{\pi^2}{2h}\epsilon_{33}\gamma=0 \tag{18c}$$

as the equilibrium equations, and the boundary conditions in Eqs. (16a-e) become

$$hC_{11}\frac{\partial u}{\partial r}+\frac{h}{r}C_{12}u+2e_{31}\gamma_0-\bar{t}_r=0 \tag{19a}$$

or $u=\bar{u}$ at $r=a$ and $r=b$

$$\left[\frac{h^3}{12}C_{11}+\frac{h}{2}\left(A_{11}-A_{12}\right)\right]\frac{\partial}{\partial r}\nabla^2 w-\frac{2h}{\pi}e_{31}\frac{\partial\gamma}{\partial r}+\bar{t}_z=0 \tag{19b}$$

or $w=\bar{w}$ at $r=a$ and $r=b$

$$\epsilon_{11}\frac{\partial\gamma}{\partial r}=0 \quad \text{or} \quad \gamma=\bar{\gamma} \text{ at } r=a \text{ and } r=b \tag{19c}$$

$$-\frac{h^3}{12}C_{11}\frac{\partial^2 w}{\partial r^2}-\frac{h^3}{12r}C_{12}\frac{\partial w}{\partial r}+\frac{2h}{\pi}e_{31}\gamma-\frac{h}{2}\left(A_{11}-A_{12}\right)\nabla^2 w-\bar{M}_\theta=0 \tag{19d}$$

or $\dfrac{\partial w}{\partial r}=\dfrac{\partial\bar{w}}{\partial r}$ at $r=a$ and $r=b$

3.2. Transversely Isotropic Piezomagnetic Circular Kirchhoff Plate Model Incorporating the Microstructure Effect

When the piezoelectric effect is neglected by setting $e_{ij}=0$, $\epsilon_{ij}=0$ and $d_{ij}=0$, Eqs. (15a-d) reduce to

$$hC_{11}\frac{\mathrm{d}}{\mathrm{d}r}\left[\frac{1}{r}\frac{\mathrm{d}}{\mathrm{d}r}(ru)\right]+f_r=0 \tag{20a}$$

$$-\left[\frac{h^3}{12}C_{11}+\frac{h}{2}\left(A_{11}-A_{12}\right)\right]\nabla^4 w+\frac{2h}{\pi}q_{31}\nabla^2\zeta+f_z=0 \tag{20b}$$

$$\frac{h}{2}\mu_{11}\nabla^2\zeta-2q_{31}\frac{h}{\pi}\nabla^2 w-\frac{\pi^2}{2h}\mu_{33}\zeta=0 \tag{20c}$$

as the equilibrium equations, and the boundary conditions in Eqs. (16a-e) yield

$$hC_{11}\frac{\partial u}{\partial r}+\frac{h}{r}C_{12}u+2q_{31}\zeta_0-\bar{t}_r=0 \tag{21a}$$

or $u=\bar{u}$ at $r=a$ and $r=b$

$$\left[\frac{h^3}{12}C_{11}+\frac{h}{2}\left(A_{11}-A_{12}\right)\right]\frac{\partial}{\partial r}\nabla^2 w-\frac{2h}{\pi}q_{31}\frac{\partial\zeta}{\partial r}+\bar{t}_z=0 \tag{21b}$$

or $w=\bar{w}$ at $r=a$ and $r=b$

$$\mu_{11}\frac{\partial\zeta}{\partial r}=0 \quad \text{or} \quad \zeta=\bar{\zeta} \text{ at } r=a \text{ and } r=b \tag{21c}$$

$$-\frac{h^3}{12}C_{11}\frac{\partial^2 w}{\partial r^2}-\frac{h^3}{12r}C_{12}\frac{\partial w}{\partial r}+\frac{2h}{\pi}q_{31}\zeta-\frac{h}{2}\left(A_{11}-A_{12}\right)\nabla^2 w-\bar{M}_\theta=0 \tag{21d}$$

or $\dfrac{\partial w}{\partial r}=\dfrac{\partial\bar{w}}{\partial r}$ at $r=a$ and $r=b$

3.3. Classical Transversely Isotropic Magneto-electro-elastic Circular Kirchhoff Plate Model

When the microstructure effect is neglected by setting $(A_{11}-A_{12})=0$, Eqs. (15a-d) reduce to

$$hC_{11}\frac{\mathrm{d}}{\mathrm{d}r}\left[\frac{1}{r}\frac{\mathrm{d}}{\mathrm{d}r}\left(ru\right)\right]+f_r=0 \tag{22a}$$

$$-\frac{h^3}{12}C_{11}\nabla^4 w+\frac{2h}{\pi}e_{31}\nabla^2\gamma+\frac{2h}{\pi}q_{31}\nabla^2\zeta+f_z=0 \tag{22b}$$

$$\frac{h}{2}\epsilon_{11}\nabla^2\gamma+\frac{h}{2}d_{11}\nabla^2\zeta-2e_{31}\frac{h}{\pi}\nabla^2 w-\frac{\pi^2}{2h}\epsilon_{33}\gamma-\frac{\pi^2}{2h}d_{33}\zeta=0 \tag{22c}$$

$$\frac{h}{2}\mu_{11}\nabla^2\zeta+\frac{h}{2}d_{11}\nabla^2\gamma-2q_{31}\frac{h}{\pi}\nabla^2 w-\frac{\pi^2}{2h}\mu_{33}\zeta-\frac{\pi^2}{2h}d_{33}\gamma=0 \tag{22d}$$

as the equilibrium equations, and the boundary conditions in Eqs. (16a-e) result in

$$hC_{11}\frac{\partial u}{\partial r}+\frac{h}{r}C_{12}u+2e_{31}\gamma_0+2q_{31}\zeta_0-\bar{t}_r=0 \tag{23a}$$

or $u=\bar{u}$ at $r=a$ and $r=b$

$$\frac{h^3}{12}C_{11}\frac{\partial}{\partial r}\nabla^2 w-\frac{2h}{\pi}e_{31}\frac{\partial \gamma}{\partial r}-\frac{2h}{\pi}q_{31}\frac{\partial \zeta}{\partial r}+\bar{t}_z=0 \tag{23b}$$

or $w=\bar{w}$ at $r=a$ and $r=b$

$$\epsilon_{11}\frac{\partial \gamma}{\partial r}+d_{11}\frac{\partial \zeta}{\partial r}=0 \quad \text{or} \quad \gamma=\bar{\gamma} \text{ at } r=a \text{ and } r=b \tag{23c}$$

$$\mu_{11}\frac{\partial \zeta}{\partial r}+d_{11}\frac{\partial \gamma}{\partial r}=0 \quad \text{or} \quad \zeta=\bar{\zeta} \text{ at } r=a \text{ and } r=b \tag{23d}$$

$$-\frac{h^3}{12}C_{11}\frac{\partial^2 w}{\partial r^2}-\frac{h^3}{12r}C_{12}\frac{\partial w}{\partial r}+\frac{2h}{\pi}e_{31}\gamma+\frac{2h}{\pi}q_{31}\zeta-\bar{M}_\theta=0$$
$$\text{or} \quad \frac{\partial w}{\partial r}=\frac{\partial \bar{w}}{\partial r} \text{ at } r=a \text{ and } r=b \tag{23e}$$

4. Example: Static Bending of a Clamped Circular Plate

To study the newly developed circular Kirchhoff plate model, a static bending problem of a solid circular plate (with $a = 0$ and $b = 20h$) is solved herein. The plate is clamped at its outer edge and subjected to a uniformly distributed constant load q pointing downward.

For static bending problems, the governing equations are consistent with Eqs. (15a-d).

In view of Eqs. (16a-e), the boundary conditions for the current circular Kirchhoff plate at its outer edge $r = b$ are given by

$$u(b)=0, \quad w(b)=0, \quad \left.\frac{\mathrm{d}w}{\mathrm{d}r}\right|_{r=b}=0, \quad \gamma(b)=0, \quad \zeta(b)=0 \tag{24a-e}$$

Besides, the following symmetry conditions need to be considered:

$$u(0)=0, \quad \left.\frac{\mathrm{d}w}{\mathrm{d}r}\right|_{r=0}=0, \quad \left.\frac{\mathrm{d}\gamma}{\mathrm{d}r}\right|_{r=0}=0, \quad \left.\frac{\mathrm{d}\zeta}{\mathrm{d}r}\right|_{r=0}=0 \tag{25a-d}$$

Obviously, the radial displacement u is uncoupled with w, γ and ζ, so that it can be calculated by solving the boundary value problem (BVP) defined by Eqs. (15a),

(24a) and (25a). According to this BVP (with $f_r = 0$), it is not hard to get that $u(r) = 0$ at any point in the plate.

The transverse displacement w, electric potential γ and magnetic potential ζ can be calculated by solving the BVP defined by Eqs. (15b-d), (24b-e) and (25b-d). The coupled high-order ordinary differential equations (ODEs) are not easy to solve by direct integration because the solutions containing modified Bessel functions are usually very complicated [27, 32, 33].

In order to deal with such difficulties, the Fourier–Bessel series [27] are adopted. Solutions for w, γ and ζ can be written as:

$$\frac{\mathrm{d}}{\mathrm{d}r} w(r) = \sum_{n=1}^{\infty} W_n J_1\left(\bar{\lambda}_{1n} r\right) \tag{26a}$$

$$\gamma(r) = \sum_{n=1}^{\infty} H_n J_0\left(\bar{\lambda}_{0n} r\right) \tag{26b}$$

$$\zeta(r) = \sum_{n=1}^{\infty} Z_n J_0\left(\bar{\lambda}_{0n} r\right) \tag{26c}$$

where $J_i(x)$ is the Bessel function of the first kind of order i, λ_{in} is the nth real zero of the function $J_i(x) = 0$, and $\bar{\lambda}_{in} = \lambda_{in} / b$. W_n, H_n and Z_n are the nth-order coefficients to be determined. Eqs. (26a-c) inherently satisfy the boundary conditions in Eqs. (24c-e) and the symmetry conditions in Eqs. (25b-d).

When considering the boundary conditions in Eq. (24b), the expression of w can be derived from integrating Eq. (26a)

$$w(r) = \sum_{n=1}^{\infty} \frac{1}{\bar{\lambda}_{1n}} W_n \left[J_0\left(\bar{\lambda}_{1n} b\right) - J_0\left(\bar{\lambda}_{1n} r\right) \right] \tag{27}$$

The uniformly distributed constant load q can be expanded as [34, 35]

$$q(r)=\sum_{n=1}^{\infty}\frac{q}{J_2\left(\lambda_{1n}\right)}J_0\left(\bar{\lambda}_{1n}r\right)\ \text{ or }\ q(r)=\sum_{n=1}^{\infty}\frac{2q}{J_1\left(\lambda_{0n}\right)\lambda_{0n}}J_0\left(\bar{\lambda}_{0n}r\right) \tag{28a, b}$$

Substituting Eqs. (26b-28b) into Eqs. (15b-d) yields

$$\begin{bmatrix}K_{11} & K_{12} & K_{13}\\ K_{21} & K_{22} & K_{23}\\ K_{31} & K_{32} & K_{33}\end{bmatrix}\begin{Bmatrix}W_n\\ H_n\\ Z_n\end{Bmatrix}=\begin{Bmatrix}Q_n\\ 0\\ 0\end{Bmatrix} \tag{29}$$

where

$$K_{11}=-\left[\frac{h^3}{12}C_{11}+\frac{h}{2}\left(A_{11}-A_{12}\right)\right]\left(\bar{\lambda}_{1n}\right)^3J_0\left(\bar{\lambda}_{1n}r\right) \tag{30a}$$

$$K_{12}=\frac{2h}{\pi}e_{31}\left(\bar{\lambda}_{0n}\right)^2J_0\left(\bar{\lambda}_{0n}r\right) \tag{30b}$$

$$K_{13}=\frac{2h}{\pi}q_{31}\left(\bar{\lambda}_{0n}\right)^2J_0\left(\bar{\lambda}_{0n}r\right) \tag{30c}$$

$$K_{21}=-2e_{31}\frac{h}{\pi}\bar{\lambda}_{1n}J_0\left(\bar{\lambda}_{1n}r\right) \tag{30d}$$

$$K_{22}=-\frac{h}{2}\epsilon_{11}\left(\bar{\lambda}_{0n}\right)^2J_0\left(\bar{\lambda}_{0n}r\right)-\frac{\pi^2}{2h}\epsilon_{33}J_0\left(\bar{\lambda}_{0n}r\right) \tag{30e}$$

$$K_{23}=-\frac{h}{2}d_{11}\left(\bar{\lambda}_{0n}\right)^2J_0\left(\bar{\lambda}_{0n}r\right)-\frac{\pi^2}{2h}d_{33}J_0\left(\bar{\lambda}_{0n}r\right) \tag{30f}$$

$$K_{31}=-2q_{31}\frac{h}{\pi}\bar{\lambda}_{1n}J_0\left(\bar{\lambda}_{1n}r\right) \tag{30g}$$

$$K_{32}=-\frac{h}{2}d_{11}\left(\bar{\lambda}_{0n}\right)^2J_0\left(\bar{\lambda}_{0n}r\right)-\frac{\pi^2}{2h}d_{33}J_0\left(\bar{\lambda}_{0n}r\right) \tag{30h}$$

$$K_{33}=-\frac{h}{2}\mu_{11}\left(\bar{\lambda}_{0n}\right)^2J_0\left(\bar{\lambda}_{0n}r\right)-\frac{\pi^2}{2h}\mu_{33}J_0\left(\bar{\lambda}_{0n}r\right) \tag{30i}$$

Then, substituting W_n, H_n and Z_n obtained in Eqs. (29), respectively, into Eqs. (27), (26b) and (26c) will give the exact solutions of the transverse displacement w, electric potential γ and magnetic potential ζ based on the current circular Kirchhoff plate model for the clamped plate subjected to the axisymmetrically distributed load.

Note that the current Fourier–Bessel series method possesses the same

limitations as those of the classical model. For an annular circular plate (with $a \neq 0$), the FEM and HDQ techniques have been successfully employed to determine the static deflections of a thin annular plate [37]. In constant to the inner radius a, the load and boundary conditions are the main factors influencing the solutions.

In order to verify the correctness of the current model, a comparative study of the deflection of the clamped circular Kirchhoff plate subjected to a uniform load between the current model and the model with couple stress effect only provided by Zhang et al. [28] are plotted in Fig. 2. For a convenient comparison, the current model is degenerated to a pure elastic model by neglecting both piezoelectric and piezomagnetic effects (i.e., $e_{31} = q_{31} = \mu_{11} = \mu_{33} = \epsilon_{11} = \epsilon_{33} = d_{11} = d_{33} = 0$). The plate parameters, geometric dimensions and boundary conditions of the two models are adopted from Zhang et al. [28], and the Young's modulus E and Poisson's ratio v for the isotropic case are related to the current elastic stiffness constant through

$$C_{11} = \frac{(1-v)E}{(1+v)(1-2v)} \tag{31}$$

From Fig. 2, it is obvious that the results of the current and classical pure elastic models are the same as those from Zhang et al. [28] This validates the current model and indicates that the couple stress effect will always lead to reduced values of the deflection, as expected.

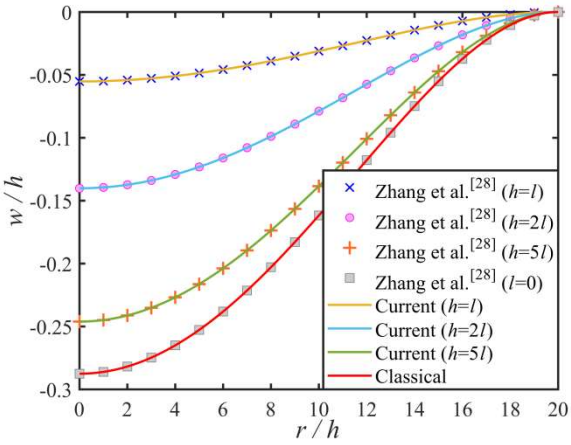

Fig. 2. Comparison of the deflection of the clamped plate subjected to a uniform load

To further study the newly derived clamped MEE circular Kirchhoff plate model, some numerical results are obtained and presented. The material of the plate is taken to be a two-phase composite $BaTiO_3$-$CoFe_2O_4$. The material properties are listed in **Table 1** [27, 36], in which v_f means the volume fraction of $BaTiO_3$. When v_f= 0%, the material turns to be a purely piezomagnetic (PM) material $CoFe_2O_4$, and when v_f= 100%, only a purely piezoelectric (PE) material $BaTiO_3$ is left. In addition, the uniformly distributed constant load q is fixed at 1 MPa.

Table 1. Effective properties of $BaTiO_3$-$CoFe_2O_4$ composite

v_f	0% (PM)	20%	40%	50%	60%	80%	100% (PE)
C_{11}	286	262	238	226	214	190	166
C_{12}	173	153.8	134.6	125	115.4	96.2	77
C_{13}	170	151.6	133.2	124	114.8	96.4	78
C_{33}	269.5	248	226.5	215.75	205	183.5	162
C_{44}	45.3	44.84	44.38	44.15	43.92	43.46	43
e_{15}	0	2.32	4.64	5.8	6.96	9.28	11.6
e_{31}	0	–0.88	–1.76	–2.2	–2.64	–3.52	–4.4
e_{33}	0	3.72	7.44	9.3	11.16	14.88	18.6

ϵ_{11}	0.08	2.30	4.53	5.64	6.75	8.98	11.2
ϵ_{33}	0.093	2.59	5.10	6.35	7.60	10.10	12.6
q_{15}	550	440	330	275	220	110	0
q_{31}	580.3	464.24	348.18	290.15	232.12	116.06	0
q_{33}	699.7	559.76	419.82	349.85	279.88	139.94	0
d_{11}	0	2.6	4.58	5.38	6.02	7.04	0
d_{33}	0	2020	2760	2740	2520	1550	0
μ_{11}	590	473	356	297.5	239	122	5
μ_{33}	157	127.6	98.2	83.5	68.8	39.4	10
ρ	5300	5400	5500	5550	5600	5700	5800
l	7.33	7.29	7.24	7.21	7.18	7.10	7.00

* Units: C_{ij}, in GPa, e_{ij}, in C/m^2, ϵ_{ij}, in 10^{-9} C^2/(N·m^2), q_{ij}, in N/(A·m), d_{ij}, in 10^{-12} Ns/(V·C), μ_{ij}, in 10^{-6} Ns^2/C^2, ρ, in kg/m^3, and l, in μm.

The couple stress stiffness constants can be written as [19]

$$A_{ij} = C_{ij} l^2 \tag{31}$$

Theoretically, the results will be more accurate as the expansion term n of Fourier Bessel series increases. After a careful study, n = 30 here is sufficient to meet the accuracy requirement.

Figures 3, 4 and 5 show the numerical results of transverse displacement w, electric potential γ and magnetic potential ζ of the current model (the newly derived model considering the microstructure effect) and the classical model (with $A_{11}-A_{12} = 0$), respectively, with v_f=50%.

It can be easily seen that all results predicted by the current model are smaller than those of the classical model. With the increase of plate thickness h, results of the current model are more and more close to the classical cases, indicating that the

microstructure effect has a significant influence on the current model when the plate thickness is very small.

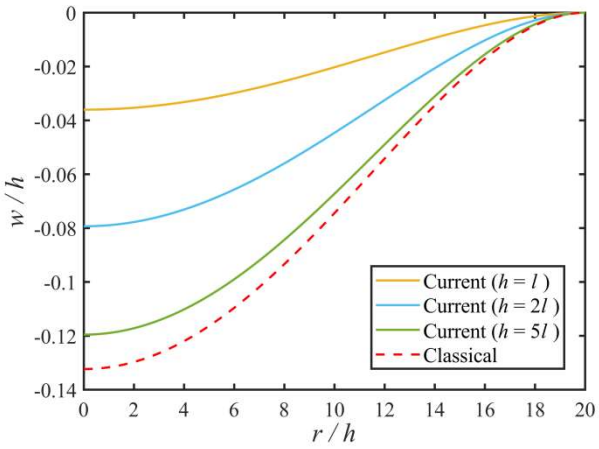

Fig. 3. The transverse displacement of the clamped circular Kirchhoff plate

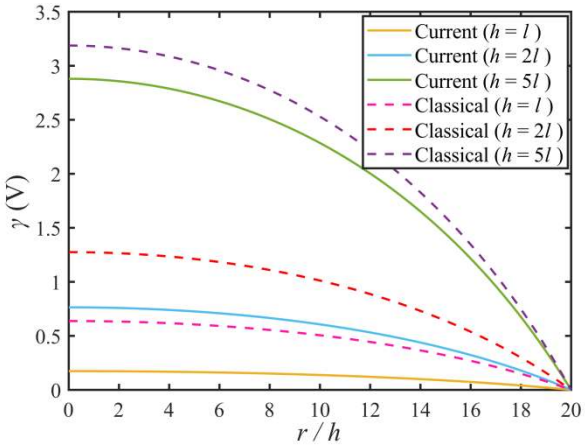

Fig. 4. The electric potential of the clamped circular Kirchhoff plate

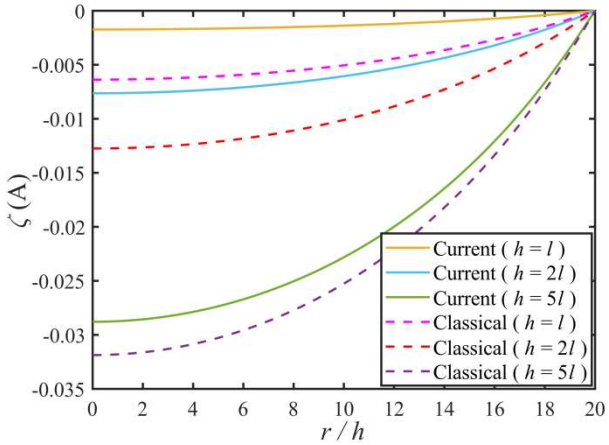

Fig. 5. The magnetic potential of the clamped circular Kirchhoff plate

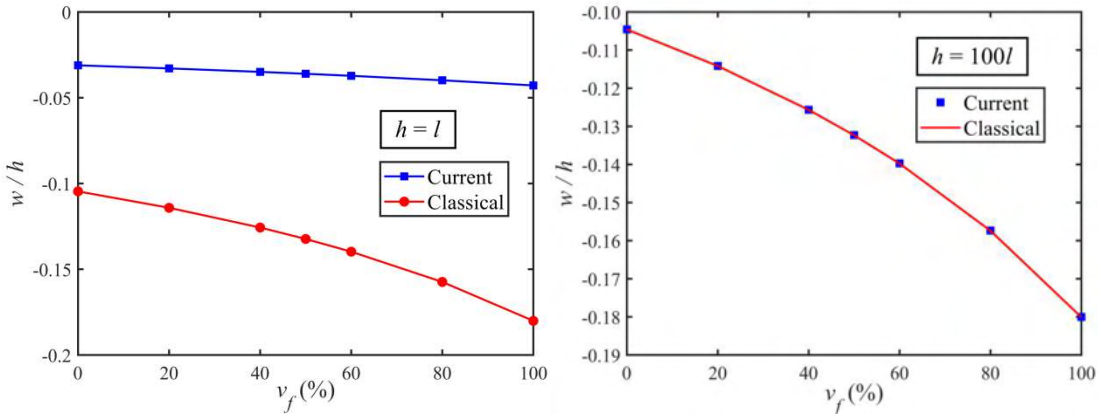

(a) (b)

Fig. 6. Transverse displacement at the central point varying as a function of v_f of the current and classical models: (a) $h = l$; (b) $h = 100l$

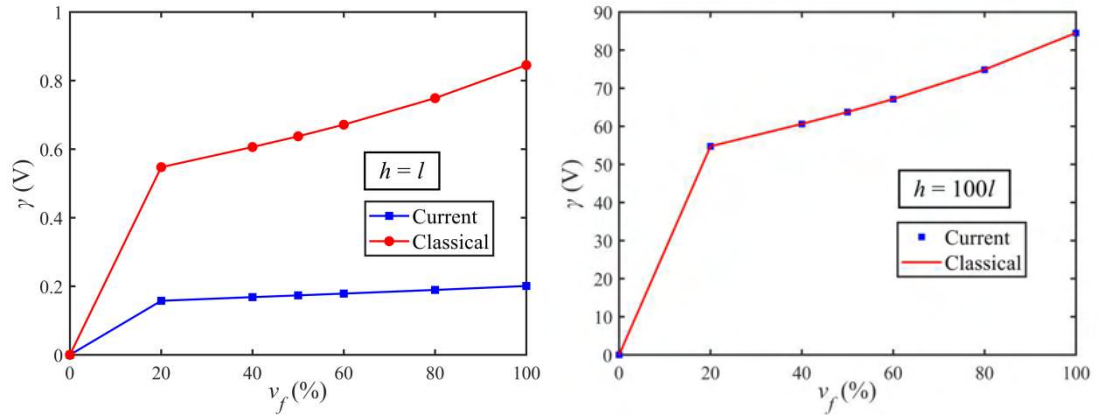

(a) (b)

Fig. 7. Electric potential at the central point varying as a function of v_f of the current and classical models: (a) $h = l$; (b) $h = 100l$

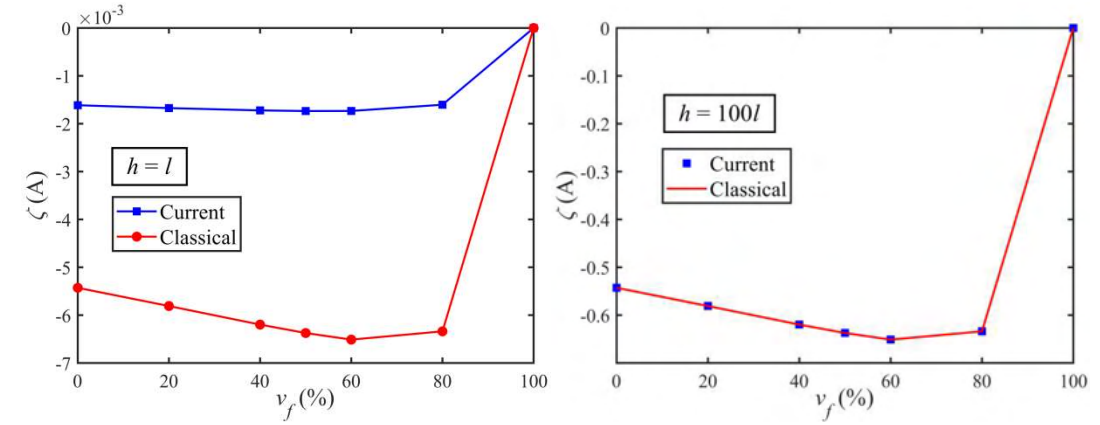

(a) (b)

Fig. 8. Magnetic potential at the central point varying as a function of v_f of the current and classical models: (a) $h = l$; (b) $h = 100l$

To study the effects of the magneto-electro-elastic coupling, the maximum transverse displacement w (deflection at the midpoint of the plate) under different v_f conditions is plotted in Fig. 6a. In addition, Fig. 7a and Fig. 8a present the electric potential and magnetic potential at the midpoint of the plate varying as a function of v_f, respectively. The blue square lines describe the results of the current model with $h = l$, and the red circular lines describe the results of the classical model with $h = l$.

From Fig. 6a, it is observed that the transverse displacements with $h = l$ predicted by both the current and classical models decrease with the increase of v_f. However, the transverse displacement given by the classical model decreases more quickly than that predicted by the current model as v_f increases. From Fig. 7a, it is shown that the electric potential of the current model increases with the increase of v_f. This variation trend is similar to that of the classical model. In addition, the electric potential of the classical model is always larger than that of the current model, as shown in Fig. 7a. From Fig. 8a, it is shown that the magnitudes of the magnetic potential of both the current and classical models gradually increase with the increase of v_f before reaching their maximum values around 60%, after which the magnetic potentials decrease with v_f for the remaining values. When the piezoelectric effect disappears, no electric potential is generated in the entire circular plate. Similarly, there is no magnetic potential generated for the plate when the piezomagnetic effect disappears, as expected.

To further illustrate this effect, Fig. 6b, Fig. 7b and Fig. 8b show the maximum

transverse displacement, the electric and magnetic potentials of the current model with $h = 100l$, which is much larger than $h = 5l$ identified in Fig. 3, Fig. 4 and Fig. 5 as a plate thickness threshold, above which the microstructure effects on these variables are negligible. These variables predicted by the classical model are also plotted and found to be the same as the current model, as shown in Fig. 6b, Fig. 7b and Fig. 8b. This finding further confirms what has been observed previously. From Fig. 6b, Fig. 7b and Fig. 8b, it is also observed that the coupling effects affect a lot for both current and classical models.

Note that the two sharp changes, as shown in Fig. 7 (with $v_f = 20\%$) and Fig. 8 (with $v_f = 80\%$), arise directly from the effective material properties of the $BaTiO_3$–$CoFe_2O_4$ composite in Table 1. This is similar to what was found in Zhang et al. [26] based on a thin magneto-electro-elastic beam model.

5. Summary

A new model for the microstructure-dependent transversely isotropic MEE circular Kirchhoff plates is developed by using the extended modified couple stress theory. The governing equations are derived via a variational method. The newly derived model can capture the microstructure-dependent size effect at the microscale.

To illustrate the new model, the static bending of a clamped transversely isotropic MEE circular plate subject to a uniformly distributed constant load is solved numerically via Fourier–Bessel series. The numerical results show that the values of transverse displacement, electric and magnetic potentials of the current model are always smaller than those of the classical model. However, with the increase of the

plate thickness h, the differences are diminishing. In addition, the numerical results show that the transverse displacement, electric and magnetic potentials vary significantly with the MEE couplings at all length scales.

Acknowledgements. The work reported here is funded by the National Natural Science Foundation of China [grant numbers 12002086 and 11672099]. These supports are gratefully acknowledged.

References

[1] Ghayesh MH, Farokhi H, Alici G. Size-dependent performance of microgyroscopes. Int J Eng Sci. 2016; 100: 99–111.

[2] Salas RA, Ramírez FJ, Montealegre-Rubio W, Silva ECN, Reddy JN. A topology optimization formulation for transient design of multi-entry laminated piezocomposite energy harvesting devices coupled with electrical circuit. Int J Numer Methods Eng. 2017;113: 1370–1410.

[3] DeVoe DL. Piezoelectric thin film micromechanical beam resonators. Sens Actuator A-Phys. 2001; 88: 263-272.

[4] Liang Y, Yang W, Yang J. Transient bending vibration of a piezoelectric semiconductor nanofiber under a suddenly applied shear force. Acta Mech Solida Sin. 2019; 32: 688–697.

[5] Hu Y, Hu T, Jiang Q. Coupled analysis for the harvesting structure and the modulating circuit in a piezoelectric bimorph energy harvester. Acta Mech Solida Sin. 2007; 20: 296–308.

[6] Yang W, Hu Y, Pan EN. Electronic band energy of a bent ZnO piezoelectric

semiconductor nanowire. Appl Math Mech-Engl Ed. 2020; 41: 833–844.

[7] Li YS, Pan E. Static bending and free vibration of a functionally graded piezoelectric microplate based on the modified couple-stress theory. Int J Eng Sci. 2015; 97: 40–59.

[8] Lim CW, He LH. Size-dependent nonlinear response of thin elastic films with nano-scale thickness. Int J Mech Sci. 2004; 46: 1715–1726.

[9] Yin L, Qian Q, Wang L, Xia W. Vibration analysis of microscale plates based on modified couple stress theory. Acta Mech Solida Sin. 2010; 23**:** 386–393.

[10] Lam DCC, Yang F, Chong ACM, Wang J, Tong P. Experiments and theory in strain gradient elasticity. J Mech Phys Solids. 2003; 51: 1477–1508.

[11] Eringen AC. On differential equations of nonlocal elasticity and solutions of screw dislocation and surface waves. J Appl Phys. 1983; 54: 4703–4710.

[12] Eringen AC. Nonlocal continuum field theories. New York: Springer-Verlag; 2002.

[13] Li YS, Cai ZY, Shi SY. Buckling and free vibration of magnetoelectroelastic nanoplate based on nonlocal theory. Compos Struct. 2014; 111: 522–529.

[14] Vinyas M, Nischith G, Loja MAR, Ebrahimi F, Duc ND. Numerical analysis of the vibration response of skew magneto-electro-elastic plates based on the higher-order shear deformation theory. Compos Struct. 2019; 214: 132-142.

[15] Reddy JN. Mechanics of laminated composite plates and shells: theory and analysis. CRC Press LLC USA; 2004.

[16] Zheng YF, Xu L-L, Chen C-P. Nonlinear bending analysis of

magnetoelectroelastic rectangular plates using higher order shear deformation theory. J Mech Sci Technol. 2021; 35: 1099–1108.

[17] Wang WJ, Li P, Jin F. Two-dimensional linear elasticity theory of magneto-electro-elastic plates considering surface and nonlocal effects for nanoscale device applications. Smart Mater Struct. 2016; 25: 095026.

[18] Ebrahimi F, Dabbagh A. On flexural wave propagation responses of smart FG magneto-electro-elastic nanoplates via nonlocal strain gradient theory. Compos Struct. 2017; 162: 281-293.

[19] Qu YL, Li P, Zhang GY, Jin F, Gao X-L. A microstructure-dependent anisotropic magneto-electro-elastic Mindlin plate model based on an extended modified couple stress theory. Acta Mech. 2020; 231: 4323–4350.

[20] Toupin RA. Elastic materials with couple-stresses. Arch Ration Mech Anal. 1962; 11: 385–414.

[21] Mindlin RD. Influence of couple-stresses on stress concentrations. Exp Mech. 1963; 3: 1–7.

[22] Tang PY. Interpretation of bend strength increase of graphite by the couple stress theory. Comput Struct. 1983; 16: 45–49.

[23] Yang F, Chong ACM, Lam DCC, Tong P. Couple stress based strain gradient theory for elasticity. Int J Solids Struct. 2002; 39: 2731–2743.

[24] Park SK, Gao X-L. Variational formulation of a modified couple stress theory and its application to a simple shear problem. Z angew Math Phys. 2008; 59: 904–917.

[25] Zhang GY, Gao X-L, Guo ZY. A non-classical model for an orthotropic Kirchhoff plate embedded in a viscoelastic medium. Acta Mech. 2017; 228: 3811–3825.

[26] Zhang GY, Qu YL, Gao X-L, Jin F. A transversely isotropic magneto-electro-elastic Timoshenko beam model incorporating microstructure and foundation effects. Mech Mater. 2020; 149: 103412.

[27] Zhou S-S, Gao X-L. A nonclassical model for circular mindlin plates based on a modified couple stress theory. J Appl Mech. 2014; 81: 051014.

[28] Zhang GY, Gao X-L, Wang JZ. A non-classical model for circular Kirchhoff plates incorporating microstructure and surface energy effect. Acta Mech. 2015; 226: 4073–4085.

[29] Ma HM, Gao XL, Reddy JN. A non-classical Mindlin plate model based on a modified couple stress theory. Acta Mech. 2011; 220: 217–235.

[30] Wang Q. On buckling of column structures with a pair of piezoelectric layers. Eng Struct. 2002; 24: 199-205.

[31] Qu YL, Zhang GY, Fan YM, Jin F. A non-classical theory of elastic dielectrics incorporating couple stress and quadrupole effects: part I – reconsideration of curvature-based flexoelectricity theory. Math Mech Solids. (published online on March 22, 2021) https://doi.org/10.1177/10812865211001533.

[32] Ariman T. On circular micropolar plates. Ing arch. 1968; 37: 156–160.

[33] Wang R, Han Q, Pan E. An analytical solution for a multilayered magneto-electro-elastic circular plate under simply supported lateral boundary conditions. Smart Mater Struct. 2010; 19: 065025.

[34] Zhang GY, Gao X-L, Tang S. A non-classical model for circular mindlin plates incorporating microstructure and surface energy effects. Procedia IUTAM. 2017; 21: 48-55.

[35] Kreyszig E. Advanced engineering mathematics. J Wiley & Sons Inc USA; 2011.

[36] Wang Y, Xu RQ, Ding HJ. Axisymmetric bending of functionally graded circular magneto-electro-elastic plates. Eur J Mech A-Solid. 2011; 30: 999-1011.

[37] Yuan X, Tian T, Zhou H, Zhou J. Comparisons of methods for solving static deflections of a thin annular plate. Appl Numer Math. 2018; 127: 266-279.